VOL. 17, NO. 10 J. AIRCRAFT OCTOBER 1980
ARTICLE NO. 80-4101

C80-124

Effect of Tip Vortex Structure on Helicopter Noise Due to Blade-Vortex Interaction

00018
00023

Sheila E. Widnall* and Thomas L. Wolf†
Massachusetts Institute of Technology, Cambridge, Mass.

A potential cause of helicopter impulsive noise, commonly called blade slap, is the unsteady lift fluctuation on a rotor blade due to interaction with the vortex trailed from another blade. The relationship between vortex structure and the intensity of the acoustic signal is investigated. Unsteady lift on the blades due to blade-vortex interaction is calculated using linear unsteady aerodynamic theory, and expressions are derived for the directivity, frequency spectrum, and transient signal of the radiated noise. The inviscid rollup model of Betz is used to calculate the velocity profile in the trailing vortex from the spanwise distribution of blade tip loading. A few cases of tip loading are investigated, and numerical results are presented for the unsteady lift and acoustic signal due to blade-vortex interaction. The intensity of the acoustic signal is shown to be quite sensitive to changes in tip vortex structures.

Nomenclature

b_0 = reference length, blade semichord
C_L = unsteady section lift coefficient
c = speed of sound
D = directivity function, Eq. (17)
h = nondimensional distance, vortex to blade in semichords
k = nondimensional acoustic wavenumber $b_0\omega/c$
k_x, k_y = wavenumber in x, y direction
L_0 = lift/unit span
M = blade normal Mach number, U/c
p = pressure
P = Fourier transform of the pressure $= (x^2+y^2+z^2)^{1/2}$, also radial coordinate in trailing vortex
$\tilde{S}$ = Strouhal frequency, $\tilde{S}=\tilde{\omega}b_0/U$
S = Doppler shifted Strouhal frequency
s_0 = blade interaction length in semichords
t' = retarded time
U_c = convection velocity along the blade
U = blade velocity
v_Θ = circumferential velocity in trailing vortex
w_0 = vertical velocity as a function of ξ, Fig. 3
W_0 = Fourier transform of vertical velocity in wavenumber σ
w = vertical velocity as function of t'
W = Fourier transform of vertical velocity in frequency $\tilde{S}$
x,y,z = Cartesian coordinate system, y also spanwise coordinate of Sec. IV
Γ_b = bound circulation on the blade
Γ_v = circulation in the trailing vortex
Λ = angle between blade and vortex, Fig. 1
ρ = fluid density
σ = wavenumber of Fourier transform in ξ, Fig. 1
Θ, Ψ = coordinate system of Fig. 2
$\tilde{\omega}$ = aerodynamic frequency, rad/s
ω = acoustic frequency, rad/s
Ω = blade passage frequency, rad/s

Received June 25, 1979; revision received Jan. 7, 1980.

Index categories: Helicopters; Noise.

*Professor, Dept. of Aeronautics and Astronautics. Member AIAA.

†Research Assistant, Dept. of Aeronautics and Astronautics. (Currently with Physical Sciences, Inc., Woburn, Mass.). Member AIAA.

I. Introduction

THE sound generated by a helicopter rotor can be categorized as either rotational or broadband noise: rotational noise is a periodic acoustic signal characterized by line spectra at the blade passage frequency and its harmonics; broadband noise is nonharmonic with a continuous spectrum. Sources of rotational noise include steady and periodic blade loading, and at high blade Mach numbers, volume displacement and nonlinear aerodynamic effects; broadband noise arises from randomly varying blade forces, due for example to atmospheric turbulence.[1]

Under certain flight conditions, helicopter rotor operation produces an impulsive, highly directional noise, repeated at the blade passage frequency, commonly referred to as blade slap. At least two mechanisms are thought to be responsible for blade slap: shock formation due to local transonic flow on the advancing blade side; and unsteady lift fluctuations on a blade caused by interaction with the tip vortex trailed from another blade. Blade-vortex interactions are more likely to occur for the case of the tandem rotor, although recent experimental evidence[2] indicates that such interactions can be an important source of noise for single rotor helicopters as well.

Widnall[3] developed a theoretical model for blade-vortex interaction in which the unsteady lift distribution computed on a two-dimensional airfoil passing obliquely over an infinite line vortex was taken as the boundary condition on a finite blade in the calculation of the acoustic farfield. This was refined by Chu[4] to incorporate sweep and fluid motion (as for a rotor in a wind tunnel). In these previous investigations, the tip vortex was modeled as a potential vortex; the viscous core was taken into account by locating the center of the vortex an "effective distance" below the blade, defined by

$$h_{\text{eff}} = \sqrt{h^2_{\text{actual}} + r^2_{\text{core}}}$$

where r_{core} is the radius of the vortex core.

The potential vortex allows an analytical treatment of the problem and gives good agreement with experiment for square tipped blades. For a blade cutting through the vortex core, experimental results show a plateauing of both pressure fluctuation on the blade and radiated noise. This effect is accurately predicted by the theory, provided r_{core} has been selected appropriately. Also the peak-to-peak pressure and general shape of the transient signal agree with experiment.

In the present study we examine the relationship between vortex structure and the acoustic pulse to identify features of

the tip vortex that make the most significant contribution to the noise signature by using the previous model to compute both the unsteady lift on the blade and the farfield acoustic signal associated with a vortex of arbitrary vorticity distribution.

The problem of predicting vortex structure given the distribution of blade loading has received considerable attention in the study of aircraft wake turbulence, where attempts have been made to predict the trailing vortex structure in the wake of an arbitrarily loaded aircraft wing. Donaldson[5] has shown that the model of Betz[6] can be successfully applied to the problem. This model is easily adapted to a numerical scheme. We apply it here to a few different loading configurations, holding the location and magnitude of the maximum blade loading constant for all cases. The choice of loading configurations is somewhat arbitrary, as little is known about the precise distribution of tip loading on helicopter blades. The examples have been selected to illustrate salient features of the model and to suggest general guidelines for design to minimize noise.

II. Unsteady Aerodynamics of Blade-Vortex Interaction

The geometry of blade-vortex interaction is depicted in Fig. 1, the blade-vortex separation is h and the angle of obliqueness Λ. All quantities are nondimensionalized by blade velocity U and semichord b_0.

We define the spatial coordinate ξ measured perpendicular to the vortex in the plane of the airfoil. Then given the distribution of circumferential velocity in the vortex, along with h and Λ, the upwash induced at the airfoil location at a given instant can be written as $w_0(\xi)$. Using Fourier transforms, $w_0(\xi)$ is represented as a distribution, in spatial wavenumber σ, of sinusoidal gusts.

$$w_0(\xi) = \int_{-\infty}^{\infty} W_0(\sigma) e^{i\sigma\xi} d\sigma$$

$$W_0(\sigma) = \frac{1}{2\pi} \int_{-\infty}^{\infty} w_0(\xi) e^{-i\sigma\xi} d\xi \tag{1}$$

As the blade passes over the vortex, the upwash pattern is convected along the span with nondimensional convection speed $U_c = 1/\tan\Lambda$. We define the nondimensional aerodynamic (Strouhal) frequency

$$\tilde{S} = \frac{\tilde{\omega} b_0}{U}$$

where we have used the tilde to distinguish the aerodynamic frequency from the acoustic frequency that appears in Sec. III.

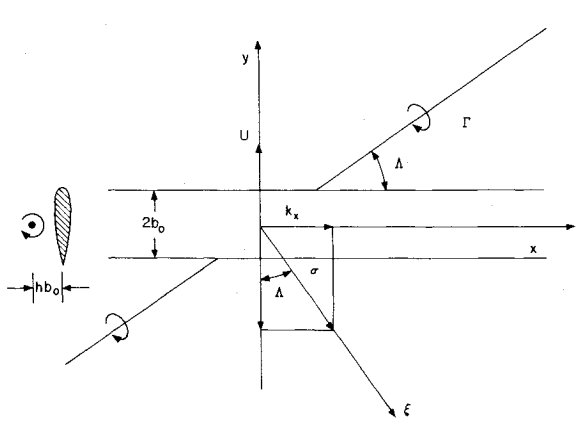

Fig. 1 Geometry of blade/vortex interaction.

The unsteady upwash $w(t')$ in blade fixed coordinates is represented as a distribution of sinusoidal gusts of frequency $\tilde{S}$.

$$w(t') = \int_{-\infty}^{\infty} W(\tilde{S}) e^{i\tilde{S}t'} d\tilde{S}$$

$$W(\tilde{S}) = \frac{1}{2\pi} \int_{-\infty}^{\infty} w(t') e^{-i\tilde{S}t'} dt' \tag{2}$$

where $t' = t - y$. We can express the upwash spectrum, $W(\tilde{S})$ of Eqs. (2) in terms of the spatial upwash wavenumber spectrum $W_0(\sigma)$ of Eq. (1). An airfoil passing over a sinusoidal gust of spatial wavenumber and experiences velocity fluctuations of frequency $\tilde{S} = \sigma\cos\Lambda$. This relation is used in Eqs. (2) to give the upwash spectrum $W(\tilde{S})$ in terms of the wavenumber spectrum $W_0(\sigma)$.

$$W(\tilde{S}) = \frac{1}{2\pi} \int_{-\infty}^{\infty} w_0(\xi) e^{-i\sigma\xi} d\xi \left(\frac{1}{\cos\Lambda}\right) = \frac{1}{\cos\Lambda} W_0(\sigma) \tag{3}$$

where, from geometry, $dt' = d\xi/\cos\Lambda$. A gust of frequency $\tilde{S}$ causes a sinusoidal lift variation along the span

$$L(x,t;\tilde{S}) = L_0(\tilde{S},\Lambda) e^{i(k_x x - \tilde{S}t)} = L_0(\tilde{S},\Lambda) e^{-i\tilde{S}t'} \tag{4}$$

where $L_0(\tilde{S},\Lambda)$ is the complex lift amplitude and $k_x = \sigma\sin\Lambda$. Since the purpose of this work is to determine the effects of tip-vortex structure upon the acoustic signature, we will use the incompressible theory of Filotas[7] to calculate the unsteady lift, as was done in Ref. 3. We are currently investigating the acoustic radiation from blade-vortex interaction at higher frequencies in a compressible flow using the more complex unsteady aerodynamic theory of Amiet.[8]

The Filotas theory gives the unsteady lift due to an oblique sinusoidal gust as

$$L_0(\tilde{S},\Lambda) = 2\pi\rho U^2 b_0^T [\,(\tilde{S}/\cos\Lambda,\Lambda)\, W(\tilde{S})\,] \tag{5}$$

where $W(\tilde{S})$ is the amplitude of a given frequency component of the input gust.

The unsteady lift at a spanwise station x in blade-fixed coordinates is found by integrating Eq. (4) over all frequencies

$$L(t') = \int_{-\infty}^{\infty} L_0(\tilde{S},\Lambda) e^{-i\tilde{S}t'} d\tilde{S} \tag{6}$$

III. Acoustic Radiation from Blade-Vortex Interaction

We now analyze the acoustic field due to blade-vortex interaction. The unsteady spanwise lift distribution previously calculated is now taken as a boundary condition on a blade of finite length in the solution of the acoustic wave equation. Fourier transforms and the method of stationary phase are used to obtain a compact expression for the acoustic farfield. This is an improved derivation over that of Ref. 3 and may be useful in similar applications.

We assume that the blade chord is smaller than a wavelength, so that the unsteady lift may be modeled as a line of acoustic dipoles, moving with velocity U in the y direction. The acoustic model is shown in Fig. 2.

The governing equation for the unsteady pressure is

$$\nabla^2 p = \frac{1}{c^2} \frac{\partial^2 p}{\partial t^2} \tag{7}$$

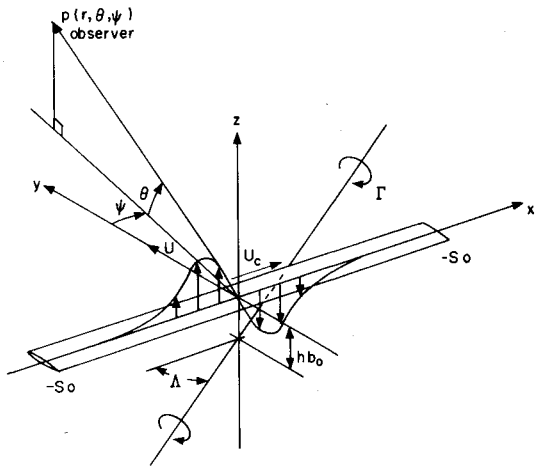

Fig. 2 Geometry of acoustic model.

We assume that the aerodynamic forces are given by Eq. (6) inside an effective blade/vortex interaction length s_0 and zero for $|x| \geq s_0$. The boundary condition may then be written

$$p^-(x,y,0) - p^+(x,y,0) = L(t-x/U_c)\delta\{b_0(y-t)\} \quad |x| \leq s_0$$

$$= 0 \qquad |x| > s_0 \tag{8}$$

The form of the boundary condition in Eq. 8 shows the lift singularities translating through the still fluid in the y direction with unit velocity and the lift pattern convecting along the span with the trace velocity U_c, dropping abruptly to zero for $|x| > s$.

We introduce the Fourier transform pair in x, y, and t

$$p(x,y,z,t) = \frac{1}{(2\pi)^3}\int_{-\infty}^{\infty}\int\int P(k_x,k_y,S;z)\,e^{ik_x x + ik_y y - iSt}$$

$$\times \mathrm{d}k_x \mathrm{d}k_y \mathrm{d}S P(k_x,k_y,S;z)$$

$$= \int_{-\infty}^{\infty}\int\int p(x,y,z,t)\,e^{-ik_x x - ik_y y + iSt}\,\mathrm{d}x\mathrm{d}y\mathrm{d}t \tag{9}$$

where S is nondimensional frequency, $\omega b_0/U$ in the acoustic reference frame.

By application of standard Fourier transform techniques, we obtain the following expression for the pressure field[9]:

$$p(x,y,z,t) = \frac{-1}{(2\pi)^2 b_0}\int_{-\infty}^{\infty}\int\int L_0(\tilde{S})$$

$$\frac{\sin\{s_0(\tilde{S}/U_c - k_x)\}}{(\tilde{S}/U_c - k_x)}\,e^{iz\sqrt{k^2-k_x^2-k_y^2}}\,e^{ik_x x + ik_y y - iSt}\,\mathrm{d}k_x\mathrm{d}k_y\mathrm{d}S \tag{10}$$

One interesting feature of Eq. (10) is that an unsteady lift of frequency $\tilde{S}$ will be perceived as sound at frequency S—the familiar doppler shift.

The pressure in the farfield is obtained by performing the integrations indicated in Eq. (10) in the limit of $\sqrt{x^2+y^2+z^2} \to \infty$. We take advantage of the farfield aymptotic behavior of the integrand to carry out the integrations over k_x and k_y, using the method of stationary phase.[9]

In general the method of stationary phase utilizes the self-canceling oscillation of an exponential factor in an integrand, allowing the contribution of the integrand to be neglected everywhere except in the neighborhood of one or more critical points.

The phase of the integrand in Eq. (10) is

$$\phi = z\{k_x \frac{x}{z} + k_y \frac{y}{z} + \sqrt{k^2 - k_x^2 - k_y^2}\} \tag{11}$$

In the limit $x,y,z \to \infty$, the oscillations in $e^{i\phi}$ become mutually self-canceling, so that contributions to the integral occur only in the vicinity of points at which the phase is stationary with respect to k_x and k_y, that is

$$\frac{\partial\phi}{\partial k_x} = \frac{\partial\phi}{\partial k_y} = 0 \tag{12}$$

Application of Eq. (12) leads to the result

$$k_x^* = k\frac{x}{r} \qquad k_y^* = k\frac{y}{r}$$

where asterisks have been used to identify k_x and k_y evaluated at the stationary point.

From geometry, k_x^* and k_y^* describe a wave that propagates radially outward from a point source. Physically, the method of stationary phase tells us that only these waves are present in the farfield limit.

Whitham[9] presents the result for application of the method of stationary phase to multiple integrations; application of this formula leads to

$$p(x,y,z,t) = \int_{-\infty}^{\infty} F(k_x^*, k_y^*, \tilde{S})\left(\frac{2\pi}{z}\right)\left(\det\left|\frac{\partial^2 W}{\partial k_x \partial k_y}\right|\right)^{-1/2}_{k_x^*,k_y^*}$$

$$\times e^{ik_x^* x + ik_y^* y - iz W(k_x^*,k_y^*,k) - i\pi/2 \mathrm{sgn}\,W^*}\,\mathrm{d}S \tag{13}$$

where

$$F(k_x,k_y,\tilde{S}) = \frac{-1}{(2\pi)^2} b_0 L_0(\tilde{S})\frac{\sin\{s_0(\tilde{S}/U_c - k_x)\}}{(\tilde{S}/U_c - k_x)}$$

$$W(k_x,k_y,k) = -\sqrt{k^2 - k_x^2 - k_y^2}$$

$$\left(\det\left|\frac{\partial^2 W}{\partial k_x \partial k_y}\right|\right)^{-1/2}_{k_x^*,k_y^*} = k\frac{z^2}{r^2}$$

and

$$\tilde{S} = S - k_y^* = S\left(1 - M\frac{y}{r}\right)$$

where the relation $k = MS$ has been used.

After some algebra, we obtain

$$p(x,y,z,t) = \frac{1}{2\pi b_0}\int_{-\infty}^{\infty} iL_0\left\{S\left(1 - M\frac{y}{r}\right)\right\}$$

$$\times \frac{\sin\left\{s_0\tilde{S}\left[\tan\Lambda\left(1 - M\frac{y}{r}\right) - M\frac{x}{r}\right]\right\}}{S\left[\tan\Lambda\left(1 - M\frac{y}{r}\right) - M\frac{x}{r}\right]}$$

$$\times \frac{z}{r^2} MS e^{iS(Mr-t)}\,\mathrm{d}S \tag{14}$$

In the coordinate system of Fig. 2, $\tilde{S}$ and S are related by

$$\tilde{S}=S(1-M\cos\theta\cos\psi) \tag{15}$$

and Eq. (14) becomes

$$p(r,\theta,\psi,t)=\frac{Ms_0}{2\pi r}\int_{-\infty}^{\infty} iL_0(\tilde{S})D(\theta,\psi,\tilde{S})$$

$$\times\tilde{S}e^{i[\tilde{S}/(1-M\cos\theta\cos\psi)](Mr/b_0-t)}\,d\tilde{S} \tag{16}$$

where $D(\Theta,\Psi,S)$ is the acoustic directivity:

$$D(\theta,\psi,\tilde{S})$$

$$=\frac{\sin\{s_0\tilde{S}[\tan\Lambda-M\cos\theta\sin\psi/(1-M\cos\theta\cos\psi)]\}\sin\theta}{-M\cos\theta\cos\psi)^2\{s_0\tilde{S}[\tan\Lambda-M\cos\theta\sin\psi/(1-M\cos\theta\cos\psi)]} \tag{17}$$

The directivity is expressed as a function of aerodynamic frequency $\tilde{S}$, in conformity with the conventional interpretation of the directivity factor as a representation of the acoustic field due to a source of prescribed frequency. For a given value of $\tilde{S}$, observed frequency S varies throughout the field, so that writing the directivity in terms of S would have been misleading. For the case of the source dimension much smaller than a wavelength ($M\tilde{S}s_0 \ll 1$), Eq. (17) is seen to reduce to the directivity factor associated with a convected point dipole

$$D(\theta,\psi)=\frac{\sin\theta}{(1-M\cos\theta\cos\psi)^2} \tag{18}$$

which applies in cases where the important blade-vortex interaction is confined to the tip region.

For effective blade-vortex interaction lengths of the order of the blade length ($M\tilde{S}s_0 \gg 1$), more likely to occur for tandem rotor blade-vortex interactions, the directivity pattern becomes highly concentrated about the Θ,Ψ combination, for which

$$\frac{\tan\Lambda}{M}-\frac{\cos\theta\sin\Psi}{1-M\cos\theta\cos\Psi}=0 \tag{19}$$

and the acoustic power is beamed strongly forward[3]; $D(\Theta,\Psi)$ of Eq. (17) reduces to $D(\Theta,\Psi)$ of Eq. (18) whenever Eq. (19) is satisfied. Note that the direction (Θ,Ψ) of maximum directivity is independent of frequency so that all wavenumber components of the input vortex will radiate maximum level to the same point in space.

The pressure field of Eq. (16) represents the signal from a single blade-vortex interaction. The helicopter signal is a repeat of this transient at the blade passage frequency. For a repeated transient, the integral of Eq. (16) is replaced by a sum at harmonics of the blade passage frequency.[3] Expressed in the frequency S heard by the acoustic observer, the pressure signature is given by

$$p_r(r,\theta,\psi,t)=i(1-M\cos\theta\cos\psi)^2\frac{Ms_0}{2\pi r}$$

$$\times\frac{\Omega b_0}{U}\sum_{m=-\infty}^{\infty}L_0\{S_m(1-M\cos\theta\cos\psi)\}D\{\theta,\psi,S_m(1$$

$$-M\cos\theta\cos\psi)\}S_m e^{iS_m(Mr/b_0-t)} \tag{20}$$

where $S_m=m(\Omega b_0/U)$.

IV. Application to Helicopter Noise Due to Blade-Vortex Interaction

The analysis presented in Secs. II and III will be applied to blade interactions with the tip vortices shed by three different assumed blade loading distributions. For the tip vortex corresponding to each of these cases, numerical results were calculated for the unsteady lift experienced by a blade interacting with the tip vortex and the associated acoustic signal over a range of interaction geometries. Helicopter parameters used to perform the computations were those of a Bell model UH-1H. Relevant specifications are (from Ref. 10): number of blades, 2; rotor diameter, 48 ft; blade semichord, 10.5 in.; average tip speed, 780 ft/s; average gross weight, 8000 lb; blade passage frequency, 65 rad/s.

Vortex Structure

It is well known that the peak levels of noise due to blade-vortex interaction are sensitive to vortex structure. Therefore, to apply Eq. (20) requires a realistic model of the tip vortex structure for a helicopter blade. We will use the Betz[6] model to predict the structure of the tip vortex.

The Betz[6] model predicts the approximate structure of a fully rolled up trailing vortex given the spanwise lift distribution on a flat wing. The model does not treat the intermediate stages between the initially flat trailing vortex sheet and the rolled up vortex; this is appropriate to the study of helicopter rotors in light of experimental evidence that vortex rollup occurs within a distance of a few blade chords.

Donaldson's results[5] suggest that only the vorticity situated between the helicopter blade tip and the position of maximum spanwise loading rolls up into the tip vortex. We assume that the maximum loading occurs at 68% of blade span,[11] and that the loading falls off monotonically to zero at the blade tip, so that only the outer 32% of blade radius contributes to tip vortex structure. The forward velocity of the blade is taken to be uniform over this length.

With reference to Fig. 3, the spanwise coordinate on the blade is y, with $y=0$ at 68% span and $y=L$ at the blade tip. The radial coordinate in the fully rolled up trailing vortex is r. We denote the spanwise distribution of bound circulation as $\Gamma_b(y)$ and the radial distribution of circulation in the vortex as $\Gamma_v(r)$.

The result of the Betz method is the determination of a function $r=r(y)$ such that $\Gamma_b(y)=\Gamma_v(r)$ at corresponding values of r and y, subject to the constraint that Γ_b and Γ_v be related by three conservation relations for two-dimensional systems assumed to apply piecewise beginning at the wing tip, to successive portions of the sheet in toward the wing root:

1) The circulation is conserved

$$\int_L^{y_1}\frac{d\Gamma_b(y)}{dy}\,dy=\int_0^{r_1}\frac{d\Gamma_v(r)}{dr}\,dr$$

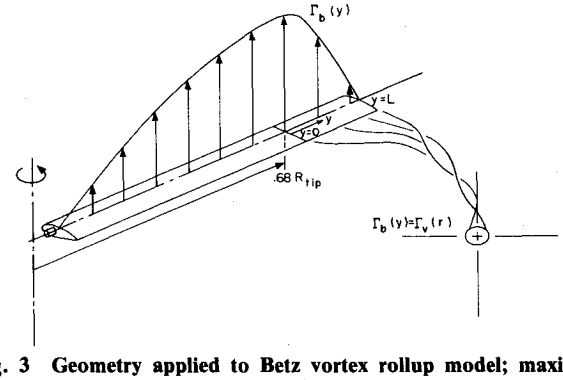

Fig. 3 Geometry applied to Betz vortex rollup model; maximum loading is assumed at 68% span, so that vorticity shed from outboard 32% span rolls up into trailing vortex.

2) The centroid of vorticity remains at a fixed spanwise location

$$\bar{y}(y_1) = \frac{1}{\Gamma_b(y_1)} \int_L^{y_1} y \frac{d\Gamma_b(y)}{dy}\, dy$$

3) The second moment of vorticity is conserved

$$\int_L^{y_1} [\bar{y}(y_1) - y]^2 \frac{d\Gamma_b(y)}{dy}\, dy = \int_0^{r_1} r^2 \frac{d\Gamma_v(r)}{dr}\, dr$$

The latter two conditions cannot be derived from fundamental theory but seem to give reasonable results for the simple situations to which they have been applied.

Rossow[12] uses the above equations to obtain the relation between r and y as

$$r = \left| \frac{1}{\Gamma_b(y)} \int_L^{y} \Gamma_b(y_1)\, dy_1 \right| \tag{21}$$

The circumferential velocity in an axially symmetric vortex is then

$$v_\theta = \frac{\Gamma_v(r)}{2\pi r} = \frac{\Gamma_b\{y(r)\}}{2\pi r} \tag{22}$$

Using Eqs. (21) and (22) it is quite straightforward to develop a numerical procedure to predict the structure of the trailing vortex, given an assumed form for the spanwise distribution of bound circulation on the blade $\Gamma_b(y)$: Eq. (21) is integrated numerically from $y=0$ to $y=L$; for each pair of values (r,y) thus found, Eq. (22) is used to evaluate the circumferential velocity $v_\theta(r)$. The vortex is assumed to be irrotational for $r>r_{max}$, so that $v_\theta \sim \Gamma/r$ for this region; v_θ is always taken to be zero at $r=0$.

To obtain an approximate value for Γ_0, maximum loading was assumed at 68% blade radius, with spanwise loading taken to fall off linearly from a maximum (L_{max}) to zero at the blade root and tip. For two 24 ft blades supporting an 8000 lb helicopter, this gives $L_{max} = 333$ lb/ft. Denoting maximum circulation by Γ_0, the relation $L_{max} = \rho U \Gamma_0$ from the lifting line theory (with U at 75% radius) gives $\Gamma_0 = 238$ ft^2/s (this estimate can of course be refined).

For a coordinate system $y=0$ at the 68% span and $y=L$ at the blade tip, three spanwise distributions of bound circulation were assumed: elliptical, $\Gamma(y) = \Gamma_0\sqrt{1-(y/L)^2}$; linear, $\Gamma(y) = \Gamma_0(1-y/L)$; and cos^2, $\Gamma = \Gamma_0 \cos^2(\pi y/2L)$. Γ_0 was taken to be the same for each.

The structure of the trailing vortex, as predicted by the Betz theory, is profoundly influenced by the slope of the loading function at the blade tip. In the case of the elliptical load distribution for which the loading falls off with infinite slope at the blade tip, a square-root singularity in circumferential velocity is predicted at $r=0$. For the cos^2 load distribution, zero slope at the blade tip leads to $v_\theta = 0$ and $dv_\theta/dr = 0$ at $r=0$, and the maximum circumferential velocity occurs at a finite distance from the vortex center. The linear load distribution has a finite nonzero slope at the blade tip, giving a discontinuous velocity at $r=0$. The circumferential velocity $v_\theta(r)$ is shown for each vortex in Fig. 4a. Although viscous effects would remove these discontinuities, even in the inviscid case a finite value for the transient acoustic signal was obtained and this is presented as a worst case.

Aerodynamic Forces and Acoustic Transients

The distribution of circumferential velocity in the trailing vortex represents the upwash encountered by a blade at zero blade-vortex separation. With an increase in blade-vortex separation, we expect two effects: the amplitude of the upwash signal is decreased as circumferential velocity falls off with an increase in distance from the vortex center; and the high frequency content of the upwash transient is diminished.

The blade would experience the most concentrated, sharply peaked upwash signal through interaction with the trailing vortex for the case of elliptical loading. A more gradual variation in upwash is experienced for the cases of linear and cos^2 loading distributions. The peak-to-peak amplitude of the upwash signal is largest for elliptical loading, less for the cos^2 case, and smallest for the case of linear loading.

To calculate unsteady lift and acoustic signal given the circumferential velocity distribution and blade-vortex separation h, we first evaluate the upwash in the plane of the airfoil $w_0(\xi)$. The Fourier transform $\tilde{W}(\sigma)$ is then computed numerically, using a fast Fourier transform (FFT) subroutine.[13] Given blade-vortex interaction angle Λ, the upwash spectrum at the airfoil location $W(\tilde{S})$ is obtained from Eq. (2) and used in Eq. (5) to give the spectrum of the unsteady lift $L_0(\tilde{S})$. The inverse transform indicated in Eq. (6) is then evaluated through the use of the FFT subroutine to give the unsteady lift due to a single blade-vortex interaction, $L(t')$.

The character of the unsteady lift signal would be expected to resemble that of the upwash signal; we found that the peak-to-peak amplitude of the unsteady lift signal was largest for the case of elliptical loading, less for the cos^2 case, and smallest for linear loading, corresponding to the relative amplitudes of the upwash signals (Figs. 4b,c,d). An increase in sweep angle Λ decreases the unsteady lift signal. The degree of harmonic distortion in the unsteady lift signal (relative to the upwash signal) is seen to increase with an increase in the high frequency content of the upwash signal, particularly evident for the case of elliptical loading at small values of h.

For the acoustic calculation, the helicopter blade is modeled as a short section of length $2s_0b_0$, representing the tip, in uniform motion with velocity U. This acoustic model was also used in Ref. 3. Although more complex acoustic models could be introduced, such as a semi-infinite blade with the unsteady loading multiplied by a tapering function to drop it to zero a short distance from the tip, the previous simple acoustic model is used since the main point of this work is to compare the effect of vortex structure on acoustic signature. At the point of maximum amplitude, these two models should differ very little. The effective blade-vortex interaction length s_0 is taken as 1/6 of the blade length (or $s_0 = 4$ ft). Effective blade velocity is taken as $0.75U_{tip}$, or $U_{eff} = 585$ ft/s, corresponding to a Mach number of 0.53. Calculations were performed for blade-vortex angle $\Lambda = 0$, 15, and 30 deg, and with blade-vortex separation distance $h = 0$, 0.2, 0.5, 1, and 2 blade semichords investigated for each value of Λ. Typical results are presented.

Observer coordinates were selected to yield the most intense acoustic signal for each case [θ_{crit} corresponding to D_{max} from Eqs. (17) and (19)]; $r = 1000$ ft was used. To obtain the acoustic transient signal, the inverse transform of the farfield spectrum [Eq. (20)] is evaluated using the FFT subroutine to give the farfield signal of a series of transients repeated at the blade passage frequency Ω.

The acoustic signal due to blade-vortex interaction is shown in Fig. 5 for various vortex structures. For each case, the acoustic field is evaluated at the θ,ψ point for which the directivity is a maximum. The time required for the acoustic signal to travel from the origin to the observer has been subtracted from the time coordinate. Figure 6 shows the peak-to-peak levels for a variety of parameters in dB re $0.0002ub$.

These results indicate that the peak acoustic signature is quite sensitive to changes in vortex structure when the blade-vortex separation distance is smaller than half the blade chord. We find, for example, that at $h=0$ the amplitude of the upwash signal associated with elliptical loading is about

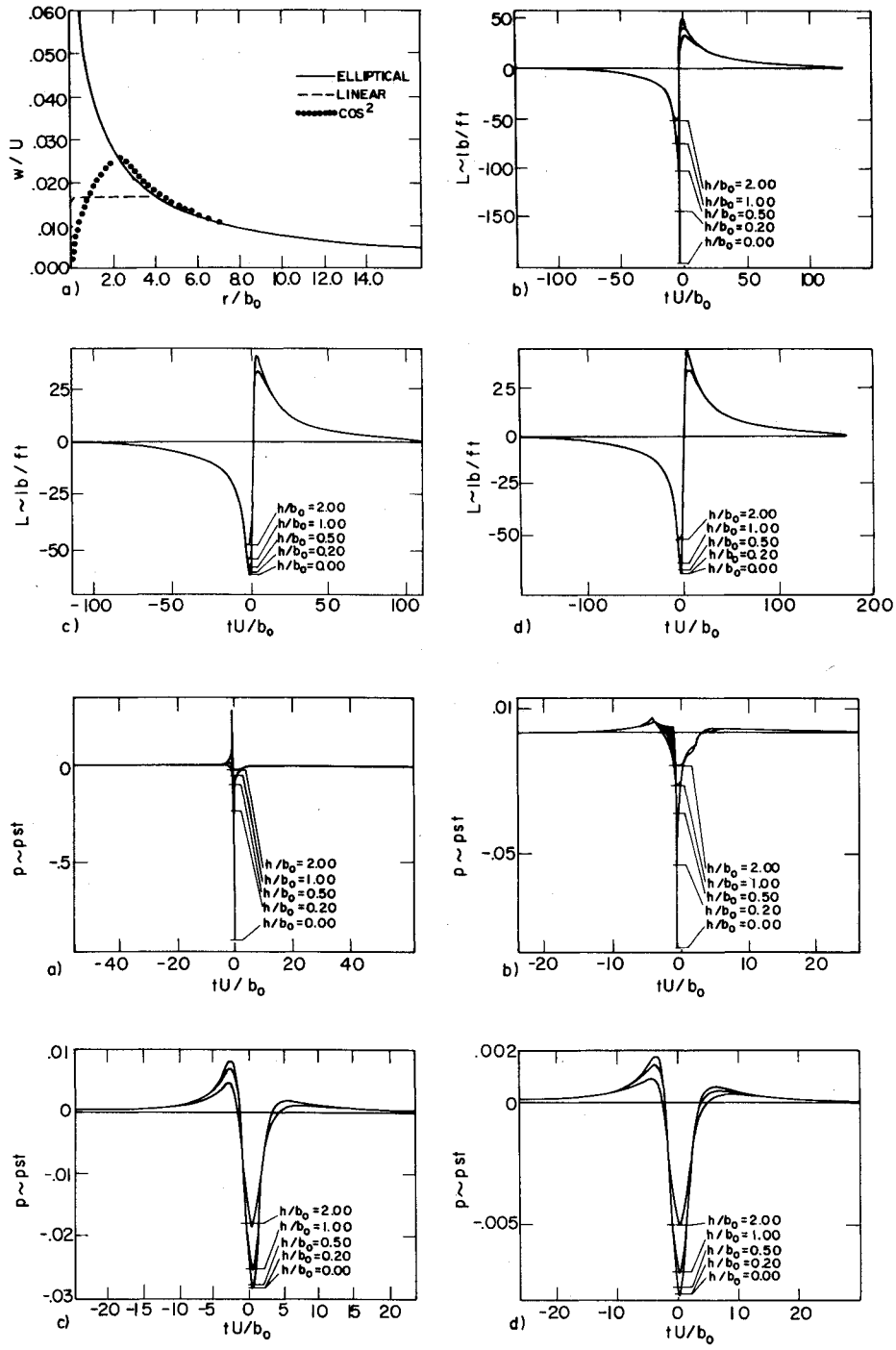

Fig. 4 Vortex velocity profiles and unsteady section lift due to blade/vortex interaction for several blade loadings; h = blade/vortex separation, $\Lambda = 0$ for all interactions: a) vortex velocity profiles; b) elliptical loading; c) linear loading; d) $\cos^2$ loading.

Fig. 5 Maximum observed transient acoustic signal due to blade/vortex interaction for several assumed blade loadings: a) elliptical loading, $\Lambda = 0$; b) linear loading, $\Lambda = 0$; c) $\cos^2$ loading, $\Lambda = 0$; d) $\cos^2$ loading, $\Lambda = 30$ deg.

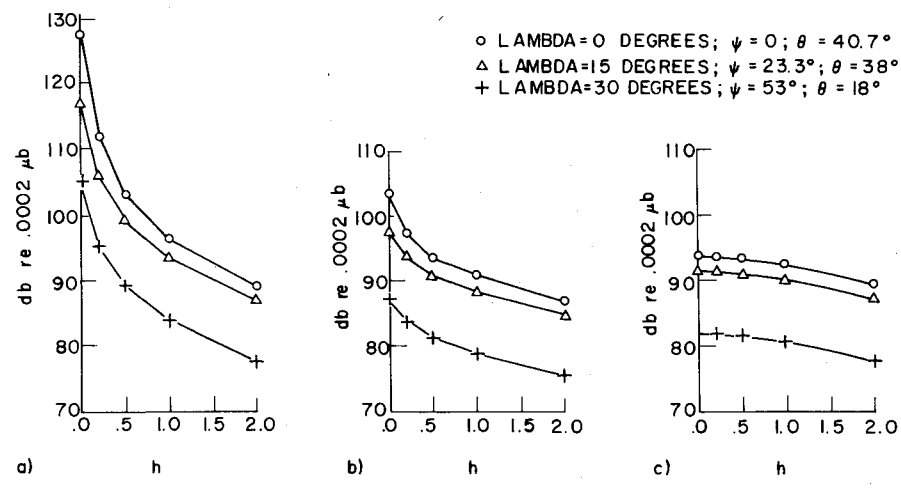

Fig. 6 Peak-to-peak pressure of transient acoustic signal for several assumed blade loadings and blade/vortex separations h: a) elliptical loading, b) linear loading, c) $\cos^2$ loading.

twice that for the $\cos^2$ case, but that the acoustic signal is 34 dB higher. This dramatic difference (corresponding to a fifty-fold increase in acoustic pressure) can be attributed to the abrupt (high frequency) character of the unsteady lift signal of the elliptical case relative to the gradual (low frequency) character of the $\cos^2$ case. Similarly, for small values of h, $\cos^2$ loading gives a signal that is 10 dB down from the corresponding linear-loading case, even though the amplitude of the unsteady lift signal for the $\cos^2$ case is larger. Of course, it must be remembered that these calculations are based upon an inviscid vortex rollup model. The presence of a viscous core would tend to diminish somewhat the high frequency content of the unsteady lift signal at very small blade-vortex separation.

The introduction of sweep causes a substantial reduction in radiated noise, as demonstrated in Figs. 5 and 6. As already indicated, an increase in Λ diminishes the high frequency content of the unsteady lift signal. A more subtle effect is the relationship between Λ and the convection speed of the lift pattern through the fluid. Since the convected Mach number of the wave along the moving blade is $M/\tan\Lambda$, the effective Mach number of the wave through the still fluid is

$$M_{\text{eff}} = \sqrt{M^2 + (M/\tan\Lambda)^2} = M/\sin\Lambda$$

so that $M = \sin\Lambda$ is the boundary between supersonic and subsonic wave speeds.

For $M < \sin\Lambda$ the only sound that is generated is due to the finite dimensions of the source: and infinite blade would radiate no sound. For this case, values of $(\theta, \psi_{\text{crit}})$ satisfying Eq. (18) do not exist; thus, no concentration of the acoustic signal occurs. As a result, the radiated noise is greatly reduced. Conversely, disturbances moving at supersonic speeds are efficient acoustic radiators, and the intensity of the peak acoustic signal increases with Mach number.

V. Conclusions and Suggestions for Further Work

Theoretical analysis of blade-vortex interaction, through the application of linear aerodynamics and acoustics of a moving source, can account for the essential role played by many of the parameters that govern the occurrence of blade slap. The extension to tip vortices of arbitrary structure provides some insight into the sensitivity of the noise signature to changes in blade tip loading and tip vortex structure. The present study indicates substantial reduction in the intensity of the acoustic signal results from control of the distribution of vorticity in the tip votex, particularly at the small blade-vortex separation.

Control of the tip vortex by alteration of blade tip shape is a potentially important method of blade slap minimization. The most significant result of this investigation with regard to tip design is that the slope of the spanwise loading distribution at the blade tip strongly influences tip vortex structure and the associated intensity of noise due to blade-vortex interaction. This result is consistent with recent experimental findings[14] that show substantial reduction in blade slap intensity through the use of a tapered (ogee) blade tip.

The present model is applicable primarily to blade-vortex interactions at small oblique angles, for which the interaction occurs over a large portion of the blade span. Such interactions are possible for tandem rotor helicopters. For single rotors, blade-vortex interactions are likely to occur at large angles for which the interaction is confined to the blade tip region. Additional theoretical modeling is required to account for the three-dimensional aerodynamic effects associated with this case.

The aerodynamic theory used here to model blade-vortex interaction applies strictly to the case of a low frequency gust in an incompressible fluid: with the low frequency assumption that the blade chord is smaller than a wavelength, we neglect chordwise pressure variation in the unsteady lift calculation and model the blade as a moving line of acoustic dipoles. At higher gust frequencies or higher Mach numbers, compressibility becomes important, and a more powerful aerodynamic model should be used for the essential details of the relationship between vortex structure and the acoustic pulse. The additional refinement obtainable from consideration of compressibility and high frequency effects was felt to be unnecessary for this initial study. The extension to include the full effects of compressibility is currently underway.

Acknowledgment

This research was supported by NASA Grant NSG-2142.

References

[1] George, A.R., "Helicopter Noise – State of the Art," AIAA Paper 77-1338, Oct., AIAA 4th Aeroacoustics Conference, Atlanta, Ga., 1977.

[2] Tangler, J.L., "The Design and Testing of a Tip to Reduce Blade Slap," Paper 963 presented at 31st Annual National Forum of American Helicopter Society, Washington, D.C., May 1975.

[3] Widnall, S.E., "Helicopter Noise Due to Blade-Vortex Interaction," *Journal of the Acoustical Society of America,* Vol. 50, No. 1 (Part 2), 1971, pp. 354-365.

[4] Chu, S., "Helicopter Noise Due to Blade/Vortex Interaction," M.S. Thesis, M.I.T., Cambridge, Mass., June 1971.

[5] Donaldson, C. duP., Snedeker, R.S., and Sullivan, R.D., "Calculation of Aircraft Wake Velocity Profiles and Comparison with Experimental Measurements," *Journal of Aircraft,* Vol. 11, Sept. 1974, pp. 547-555.

[6] Betz, A., "Behavior of Vortex Systems," NACA TM 713, 1932.

[7] Filotas, L.T., "Theory of Airfoil Response in a Gustly Atmosphere-Part I, Aerodynamic Transfer Function," UTIAS Rept. 139, University of Toronto, Canada, Oct. 1969.

[8] Amiet, R.K., "High Frequency Thin Airfoil Theory for Subsonic Flow," *AIAA Journal,* Vol. 14, Aug. 1976, pp. 1076-1082.

[9] Whitham, G.B., *Linear and Nonlinear Waves,* John Wiley and Sons, New York, 1973, p. 382.

[10] Wolf, T., "The Effect of Vortex Structure on Helicopter Noise Due to Blade/Vortex Interaction," M.S. Thesis, M.I.T., Dept. of Aeronautics and Astronautics, Cambridge, Mass., 1978.

[11] Scully, M.P., "Computation of Helicopter Rotor Wake Geometry and its Influence on Rotor Harmonic Airloads," Ph. D. Thesis, M.I.T., Cambridge, Mass., June 1971.

[12] Rossow, V.J., "On the Inviscid Rolled-Up Structure of Lift Generated Vortices," *Journal of Aircraft,* Vol. 10, Nov. 1973, pp. 647-650.

[13] Cooley, J.W., Lewis, P.A.W., and Welch, P.D., "The Fast Fourier Transform Algorithm and its Applications," IBM Research Paper RC-1743, Feb. 1967.

[14] Mantay, W.R., Shidler, P.A., and Campbell, R.L., "Some Results of the Testing of a Full-Scale Ogee Tip Helicopter Rotor; Acoustics, Loads, and Performance," AIAA Paper 77-1340, AIAA 4th Aeroacoustics Conference, Atlanta, Ga., Oct. 1977.